Available online at www.sciencedirect.com
ScienceDirect
Nuclear Instruments and Methods in Physics Research A 568 (2006) 904–911
NUCLEAR INSTRUMENTS & METHODS IN PHYSICS RESEARCH Section A
www.elsevier.com/locate/nima

Pulse shape analysis of signals from BaF_2 and CeF_3 scintillators for neutron capture experiments

S. Marrone[a,*], E. Berthomieux[b], F. Becvar[c], D. Cano-Ott[d], N. Colonna[a], C. Domingo-Pardo[e], F. Gunsing[b], R.C. Haight[f], M. Heil[g], F. Käppeler[g], M. Krtička[c], P. Mastinu[h], A. Mengoni[i,j], P.M. Milazzo[k], J. O'Donnell[f], R. Plag[g], P. Schillebeeckx[l], G. Tagliente[a], J.L. Tain[e], R. Terlizzi[a], J.L. Ullmann[f]

[a]*Dipartimento di Fisica and INFN sez. di Bari, Bari, Italy*
[b]*CEA/Saclay, Gif-sur-Yvette, France*
[c]*Charles University, Prague, Czech Republic*
[d]*CIEMAT, Madrid, Spain*
[e]*Istituto de Física Corpuscolar, CSIC-Universidad de Valencia, Spain*
[f]*Los Alamos National Laboratory, Los Alamos, USA*
[g]*Forschungszentrum Karlsruhe, Institut für Kernphysik, Karlsruhe, Germany*
[h]*INFN Laboratori di Legnaro, Legnaro (Pd), Italy*
[i]*IAEA, Wien, Austria*
[j]*CERN, Geneva, Switzerland*
[k]*INFN Sez. di Trieste, Trieste, Italy*
[l]*CEC-JRC-IRMM, Geel, Belgium*

Received 6 June 2006; received in revised form 26 July 2006; accepted 16 August 2006
Available online 12 September 2006

Abstract

The scope of this work is to study the characteristics of BaF_2 and CeF_3 signals using fast digitizers, which allow the sampling of the signal at very high frequencies and the application of the fitting method for analysis of the recorded pulses. By this procedure particle identification and the reconstruction of pile-up events can be improved, while maintaining the energy and time-of-flight resolution as compared to traditional methods. The reliability of the technique and problems connected with data acquisition are discussed with respect to accurate measurements of neutron capture cross-sections.

PACS: 29.30.Kv; 29.40.Mc; 29.85.+c; 28.20.−v

Keywords: Flash-ADC; Pulse shape discrimination; Inorganic scintillators; Neutron capture

1. Introduction

New concepts in nuclear technology for energy production and radioactive waste transmutation [1] require accurate neutron cross-sections for a large number of isotopes, in particular for radioactive isotopes or for nuclei with very small cross-sections. Precise data for neutron cross-sections are also necessary in nuclear astrophysics for understanding the relative contributions of the rapid and slow stellar neutron capture processes (known as *r*- and *s*-processes) that dominate the production of heavy elements in the universe [2]. In addition, accurate data on neutron cross-sections are also crucial for nuclear structure studies [3]. These interests have stimulated the development or upgrading of pulsed spallation neutron sources at many large-scale facilities or installations, specifically at the CERN proton synchrotron (the n_TOF facility),

*Corresponding author. Tel.: +39 080 5442511; fax: +39 080 5442470.
E-mail address: stefano.marrone@ba.infn.it (S. Marrone).

0168-9002/$ - see front matter © 2006 Elsevier B.V. All rights reserved.
doi:10.1016/j.nima.2006.08.064

the LANSCE facility in Los Alamos, the SNS facility in Oak Ridge, and the J-PARC complex in Tokai, Japan.

The relevant parameters in neutron time-of-flight experiments are the energy and time of the recorded events as well as the possibility of performing particle identification and pile-up correction. The large data rates typical of experiments with very high instantaneous neutron fluxes of powerful spallation sources often overstrain traditional data acquisition systems. An effective solution to this problem is to record the entire waveform of the detector signal with fast digitizers [4] and to process this information off-line.

Concerning the detectors, new 4π γ-ray calorimeters for the measurement of neutron capture cross-sections have been completed at the n_TOF facility [5] and at LANSCE [6], which are similar to the set-up in use at Karlsruhe [7]. The prompt γ-ray cascade produced in neutron capture reactions is detected in a segmented "soccer-ball" array subtending the entire solid angle around the sample. Although BaF_2 scintillator crystals have been used in all these calorimeters, other inorganic scintillators such as CeF_3 or BGO have been considered as well [7–9]. In particular, CeF_3 is a valid substitute to BaF_2 since it produces faster signals [9], exhibits comparable efficiency and is characterized by a smaller neutron sensitivity. The scope of the present paper is to study the properties of scintillation light (pulse shape) of heavy inorganic scintillators read out with Flash Analogue to Digital Converters (FADC) [10–14]. Emphasis is placed on the corrections for pile-up and particle identification and on the comparison of the energy and time resolution that can be achieved with BaF_2 and CeF_3 crystals.

Following a brief description of the experimental set-up and of the properties of BaF_2 and CeF_3 crystals in Section 2, the fitting procedure is described in Section 3, and the results are presented in Section 4.

2. Experimental set-up

The size of the BaF_2 and CeF_3 crystals used in this work are rather different. Therefore, different set-ups have been employed in the measurements reported here. BaF_2 and CeF_3 are attractive scintillators for neutron experiments due to their high efficiency for γ-rays and their relatively small average neutron capture cross-sections. Their scintillation properties are well known [9]. The light output of both scintillators has two main components (Table 1). Due to the shorter light component of 0.6 ns, BaF_2 is better suited for fast timing applications, whereas the long second component complicates pile-up corrections (Fig. 1). Since the scintillation light of BaF_2 is emitted in the UV, it requires the use of expensive photomultipliers with quartz windows, whereas the scintillation light of CeF_3 (Fig. 2) is emitted in the visible. In addition, CeF_3 has the advantage of smaller neutron sensitivity. In this case, problems arise from the rather poor light output (Table 1) and from the difficulty to manufacture crystals larger than 100 cm^3 in size. Finally, both scintillators contain traces of radioactivity, in particular the radium isotopes ^{226,228}Ra and their daughters.

Table 1
Scintillator properties [9]

Scintillator	Density (g/cm^3)	Light component	Decay time (ns)	Wavelength (nm)	Light output (Photons/MeV)
CeF_3	6.16	Fast	3	300	200
		Slow	27	340	4300
BaF_2	4.88	Fast	0.6	180	1800
		Slow	630	310	10,000

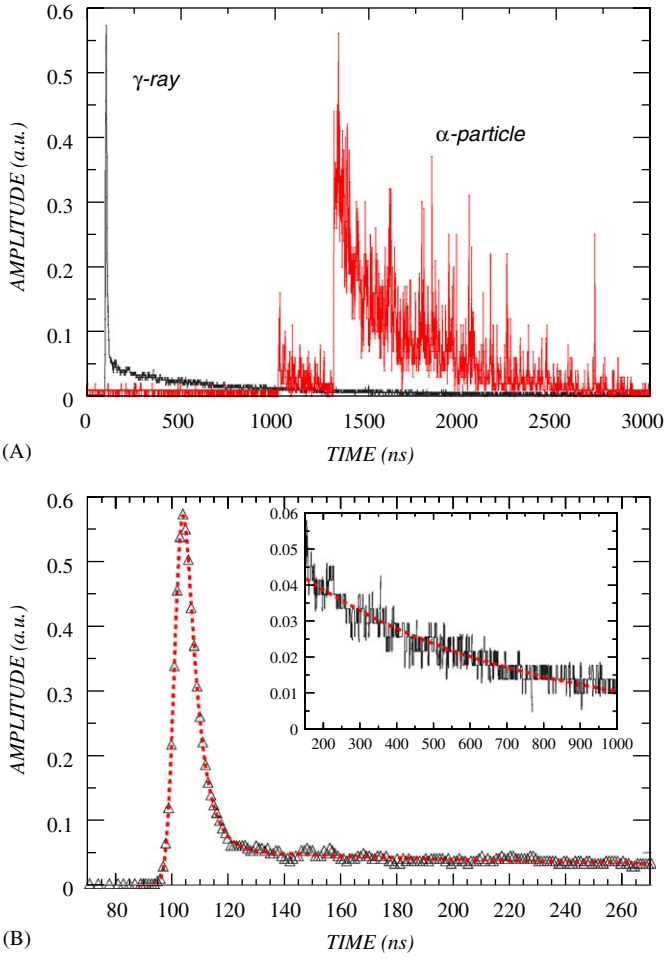

Fig. 1. Top: Typical BaF_2 signals of γ-rays and α-particles (solid curve) recorded with a FADC. Bottom: Fit of the γ-ray signal using the convoluted function of Eq. (3) (dashed curve). The inset shows the fit of the slow component with Eq. (1), illustrating the discrete sampling of the FADC-channels. It has to be noticed that the 80% of the light yield is produced by the slow component of the scintillation light (Table 1).

The present tests have been performed with a BaF_2 crystal in the form of a 15 cm long truncated regular hexagonal pyramid with 5.58 cm side length at the base and 2.97 cm at the top. This crystal was connected to an Electron Tube photomultiplier 9921B [15] (for details see Table 2). The anode pulses of the photomultiplier (PMT)

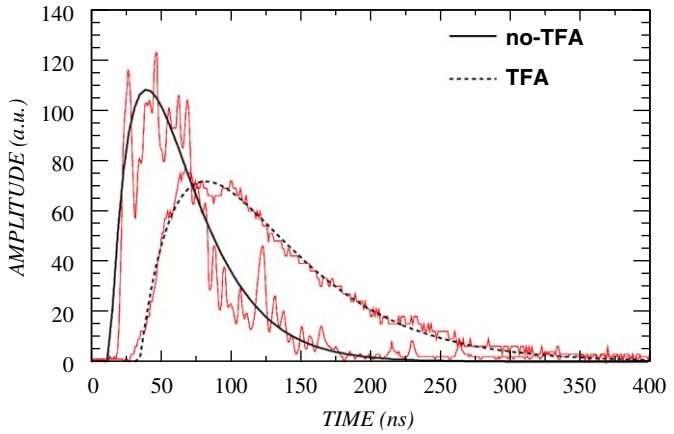

Fig. 2. Comparison of a typical CeF_3 signal (solid thin curve) recorded with a FADC and the fit with Eq. (2.1) (solid thicker curve) with the signal processed with a Timing Filter Amplifier (TFA) (broader signal and dashed curve).

Table 2
Characteristics of the phototubes [15–16]

Photo-multipliers	Rise time (ns)	Pulse width (ns)	Transit time (ns)	Jitter (ns)	Cathode diameter (mm)	Gain	Quantum efficiency (%)
Photonis XP1911	2.4	3.8	23	1.5	19	10^4–10^7	25
Electron Tube 9921B	2.1	3.2	38	2.2	67	10^3–10^6	30

were directly fed into an Acqiris FADC model DC240 [4] operated with a sampling rate of 1 GigaSamples/s (GS/s) and 8 bits dynamic range. Each signal was digitized in 3000 samples corresponding to a time window of 3 μs. The data were recorded and processed with a 500 MHz PC under Windows NT.

The CeF_3 crystal is a block $4 \times 4 \times 5\,cm^3$ in size coupled to a Photonis XP1911 photomultiplier [16] with similar properties as the Electron Tube model. The anode signals were recorded with an Acqiris FADC model DP110 with the same rate of 1 GS/s and 8 bits dynamic range. In this case 400 samples per signal were sufficient because of the shorter CeF_3 signals. For those tests, a Timing Filter Amplifier (ORTEC Model 863) with integration constant of 20 ns was used. The TFA is particularly useful to shape the pulses so to optimize the signal-to-noise ratio especially for timing measurements.

The results of this work refer to the data recorded with γ-ray sources of: ^{24}Na, ^{60}Co, ^{137}Cs, and $^{238}Pu/^{13}C$. The data used for particle identification, as discussed in Section 4.2, were obtained with neutrons produced via the $^{9}Be(p,n)^{9}B$ reaction using 2.5 MeV protons from the Van de Graaff accelerator of INFN Legnaro and with α-particles from a ^{214}Po source.

Concerning the data acquisition, commercially available FADC [4] exhibit a maximum sampling rate of 5 GS/s, corresponding to time steps of 200 ps, and 8 bit dynamic range (record length of 4 Megasamples or more), well suited for the analysis of most nuclear physics experiments. While the fast digital sampling techniques lead to a significant reduction of conventional electronics, these systems are demanding in terms of data storage and computer power for analyzing large sets of data. The important advantage of this approach is the possibility to deduce all physical information contained in the registered signals by repeated and refined off-line analyses. In addition, dead time can be minimized down to few hundreds of nanoseconds while it is much higher (~3 μs) in traditional data acquisition systems.

Finally, all recorded data were transferred to an Athlon 1600 MHz PC and analyzed with the analysis package ROOT-4.04 [17]. The routine used for the fitting method is TMINUIT class, the C++ version of the Fortran code MINUIT [18].

3. Data analysis

The advantage of using FADCs, i.e. the possibility of preserving the entire waveform for repeated and flexible data analysis, has to be traded with the need to store and to handle a large amount of data. In this section, a general approach to the analysis of FADC data and the application of the fitting method is described to extract the most accurate information and to reduce the amount of raw data.

3.1. General analysis

In the first step of data analysis, real events should be discriminated from noise and background. For the BaF_2 signals shown in Fig. 1, the derivative method for noise rejection is used. The points where the first derivative changes from zero to non-zero values correspond to the start, the peak, and the end samples of a signal. These values allow the determination of the baseline, the pulse height, and the total area under the signal which is proportional to the total charge collected in the photomultiplier. The baseline is calculated by averaging a given number of samples preceding the signal (the so-called pre-samples). Electronic noise and background events are discriminated by a two-dimensional cut in amplitude and area. It has to be noted that FADCs exhibit a small integral non-linearity and occasional baseline drifts. Both features need to be continuously monitored because they strongly affect the results.

For CeF_3 signals, the analysis is performed analogously. A typical CeF_3 signal is shown in Fig. 2 with and without the shaping performed with a timing filter amplifier (TFA). After the determination of the peak, the start and the end of the signal are evaluated. Since the duration of the CeF_3 signal is much shorter (300 ns) with respect to the BaF_2 one (see Figs. 1 and 2), it is more reliable to determine the baseline by averaging the last 50 samples of each pulse. Noise and background are again

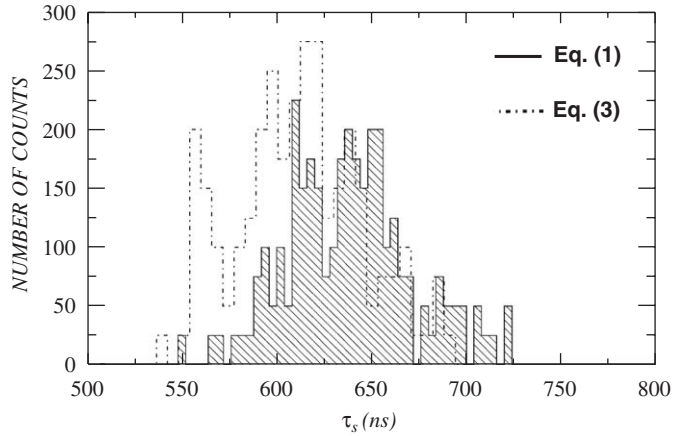

Fig. 3. Distribution of the decay time of the slow component (τ_s) in the BaF_2 signal obtained with the fitting method using Eq. (1) (hatched histogram) compared to fits with the convoluted function of Eq. (3) (dashed line).

discriminated by applying a two-dimensional cut in amplitude and area.

3.2. Fitting method

The main features of the fitting procedure are described in the literature [10–14]. In particular in a similar study of signals from liquid organic scintillators [10], we have illustrated in detail the steps for the accurate determination of the fit parameters. Therefore, the present discussion is focused on the specific features of the BaF_2 and CeF_3 analysis.

The time dependence of each light component can be expressed by an exponential:

$$L_i(t) = \frac{A_i}{\tau_i} \exp(-t/\tau_i), \tag{1}$$

where τ_i is the decay constant of the light, A_i is proportional to the light output (area of the signal), and i is the label for the fast (f) or the slow (s) light component. While this relation describes only the scintillation light, the response of the photomultiplier has to be considered in a realistic fit as well. In a first approach, the photomultiplier is represented as an equivalent RC circuit coupled to the scintillation light from the crystal [19]. For the case of a single decay constant, the solution of the differential equation for the circuit is:

$$L(t) = \frac{A_s}{\tau_s} \exp\left[-(t-t_0)/\tau_s\right] + \frac{A_R}{\vartheta} \exp\left[-(t-t_0)/\vartheta\right]. \tag{2.1}$$

For a two component scintillator one obtains correspondingly:

$$L(t) = \frac{A_s}{\tau_s} \exp\left[-(t-t_0)/\tau_s\right] + \frac{A_f}{\tau_f} \exp\left[-(t-t_0)/\tau_f\right] + \frac{A_R}{\vartheta} \exp\left[-(t-t_0)/\vartheta\right], \tag{2.2}$$

with τ_s and τ_f denoting the decay constants, ϑ the inverse of RC constant, A_s, A_f, and A_R the relative light yields, and t_0 the starting point of the fit interval.

The resolution effects of the photomultiplier (rise time, jitter, and pulse width) are not completely taken into account by Eqs. (2.1) and (2.2). To reproduce in the best way the signal in output, the most correct approach is to convolute $f(t)$, the function describing the scintillation light coming from the crystal, with $g(t)$, the response function of the photomultiplier. Provided that the photomultiplier response to a light pulse is a Gaussian with variance σ, and that $f(t)$ has the same structure of Eqs. (2.1) or (2.2), the resulting signal is:

$$L(t) = \int_{-\infty}^{+\infty} f(\tau) g(t-\tau)\, d\tau = \sum_{i=0}^{n} \left[\frac{A_i}{2\tau_i} \exp\left(\frac{\sigma^2}{2\tau_i^2} - \frac{t-t_0}{\tau_i} \right) \times \operatorname{erfc}\left(\frac{\sigma}{\sqrt{2}\tau_i} - \frac{t-t_0}{\sqrt{2}\sigma} \right) \right], \tag{3}$$

where the sum is performed over the number of light components n plus the RC constant of the circuit, erfc is the complementary error function, and A_i are the relative normalization constants, which satisfy the condition:

$$A_0 = 1 - \sum_{i=1}^{n} A_i.$$

The assumption of a Gaussian response of the photomultiplier is very common and takes all effects of the light detection and of the electronic multiplication process into account [20]. Moreover, Eq. (3) is valid in the general case of $f(t)$ having n light components and not only one as in Eq. (2.1) or two as in the Eq. (2.2).

After the analytical function and the relative parameters are identified, the whole data set is fitted using the least-square method to extract the average value and the uncertainty for each parameter. Up to six free parameters can be used for the fitting functions in Eq. (3), but this number should be reduced in order to stabilize the solutions and to speed up the minimization procedure. The best approach is to keep the well-known time constants of the scintillation light fixed and to change only the normalization constants, which are mainly determined by the particle energy. If the procedure is working properly, the extracted parameters have to be consistent with the real physical quantities (i.e. with the decay constants of the scintillation light and with the time constant of the circuit). To select the best conditions for the fitting procedure, we have compared the reduced chi-square values

$$\chi^2_{ndf} = \frac{\chi^2}{N},$$

where N is the number of degrees of freedom. In the chi-square determination, the uncertainity of the experimental data is due to the electronic noise and therefore is assumed identical for each sample. The time ranges used for the different fitting functions are 2.5 μs and 300 ns for BaF_2

and CeF_3, respectively. The chi-square tests have evidenced that the fitting curves and relative parameters depend mainly on the number of samples used in the interpolation, on the starting point (t_0), and especially on the number of free parameters set in the equations. With the proper choice of these quantities low chi-square are achieved and the signals are well reproduced by the fits. At the same time the parameters, extracted from the fit, have a reasonable physical meaning.

3.3. BaF_2 signals

The fit of BaF_2 signals with Eqs. (2.1) or (2.2) does not converge because of problems related to the pulse height resolution of the photomultiplier, to the dynamic range of the FADC, and to fluctuations of the signal, especially due to the detection of single photoelectrons. The fast component of the scintillation light is strongly affected by the resolution of the photomultiplier and by fluctuations, while the slow component depends on the sensitivity of the FADC. Therefore, the fast and slow components were fitted separately. As illustrated in Fig. 1, satisfactory results are obtained by describing the slow component with the function of Eq. (1). The slow component of the scintillation light (τ_s) was determined for the entire data set, yielding the distribution indicated by the hatched area in Fig. 3. The extracted average values and the uncertainties are given in Table 3. The relative normalization constant was treated as a free parameter and depends on the deposited energy of the detected event.

The signals can also be reproduced by using the convoluted function of Eq. (3) with two or three exponential tails. The results are reasonable in both cases, but in the fit with three exponentials the parameters of the second and third components are almost identical. Since these parameters are strongly correlated, the convoluted two-exponential function was preferred further on in the analysis using the six parameters A_s, σ, ϑ, t_0, τ_s, and A_0. However, the fit with six free parameters is time consuming and may not always converge to the best solution [10]. The fitting procedure was, therefore, stabilized by reducing the number of free parameters. This was achieved by deriving average values from the respective distributions and keeping them fixed in the fits. An example is given in Fig. 3, where the τ_s is extracted via Eqs. (1) and (3). By the same method the parameters A_s, σ, ϑ, and t_0 were defined as well, and, only A_0 was kept as a free parameter since it is determined by the energy of the individual events. The average parameters, listed in Table 3 are consistent with the nominal values of the physical quantities (Table 1). Also the variance of the Gaussian response (2.51 ± 0.91 ns) agrees well with the pulse width expected from the characteristics of the photomultipliers (Table 2).

3.4. CeF_3 signals

The CeF_3 signals differ from the BaF_2 signals, partly due to the properties of the emitted light (see Table 1) and partly because of the characteristics of the photomultipliers (the RC constant is larger see Table 3). For those reasons, the fit using Eq. (3) does not yield accurate results. Moreover since the XP1911 exhibits low quantum efficiency, the signals show large fluctuations (Fig. 2). This feature leads to problems in the determination of electronic noise and other background. Therefore, the CeF_3 signals were acquired with and without a TFA with 20 ns integration and zero differentiation constants (Fig. 2). The fits were performed with the function of Eq. (2.1) and using the same strategy as in the BaF_2 case. The average values of the parameters obtained in this way, are listed in Table 3. It can be noticed that the time constant ϑ depends on the integration constant of the TFA and on the RC constant of the photomultiplier, and is quite different with respect to the value determined for BaF_2.

In summary, the parameters extracted by the fitting procedure are consistent with the physical quantities of scintillators and photomultipliers. The fit of the fluctuating data is definitively worse than the results obtained from the smoothed signals, and time-consuming fits with a higher number of free parameters are usually less accurate.

4. Results

4.1. Pulse height and time-of-flight

The pulse height and time-of-flight information are the most important results of signal analysis in TOF measurements. The area of the signal, which corresponds to the total charge, is related to the pulse height and can be calculated either by summing the digitized wave form sample by sample or by reproducing the wave form analytically by means of the fit function. The corresponding results are compared in Fig. 4 for the exponential and

Table 3
Parameters extracted from the fitting functions

Signal	Fit function	t_0 (ns)	σ (ns)	ϑ (ns)	A_s	τ_s (ns)
BaF_2	Eq. (1)	—	—	—	—	638 ± 30
BaF_2	Eq. (3)	100 ± 4	2.51 ± 0.91	4.72 ± 0.54	0.82 ± 0.02	612 ± 40
CeF_3 (no TFA)	Eq. (2.1)	17 ± 2	—	21.4 ± 3.4	7926 ± 964	20.6 ± 5.1
CeF_3 (with TFA)	Eq. (2.1)	16 ± 1	—	50.1 ± 3.3	107 ± 10	23.6 ± 1.0

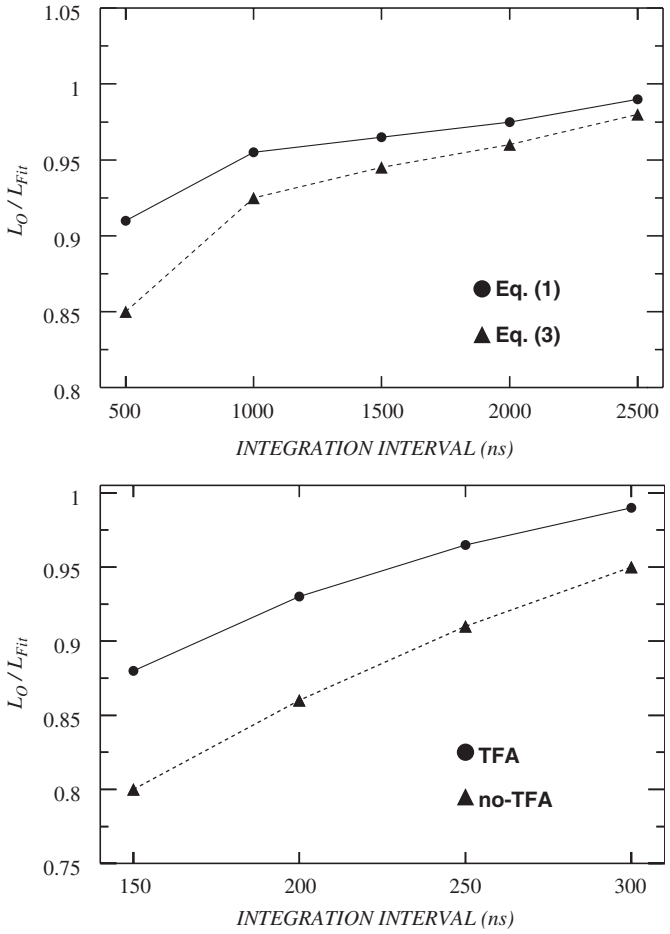

Fig. 4. Ratio of the signal areas obtained by summing the FADC samples (L_O) and by the respective fitting methods (L_{Fit}) for BaF_2 (top) and CeF_3 (bottom) as a function of the integration interval. For the CeF_3 data, the fit is performed with Eq. (2.1).

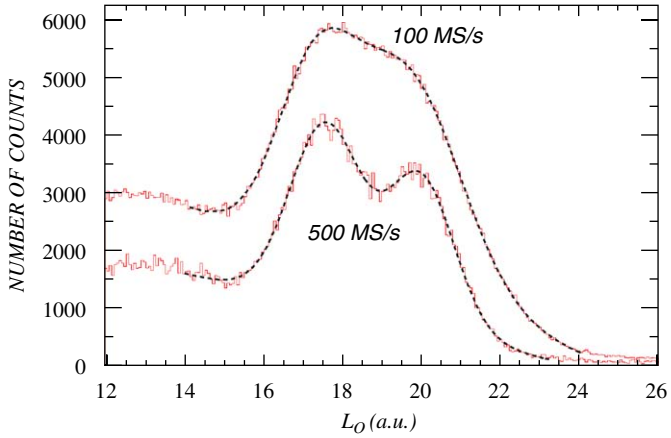

Fig. 5. Energy spectra of a BaF_2 crystal measured with a ^{60}Co source at sampling rates of 100 and 500 MS/s. The dashed curves are fits of the histograms with a sum of two Gaussian terms plus a third degree polynome representing the background. The energy resolution (see Table 4) is obtained averaging the values of both peaks.

Table 4
Energy resolution of a BaF_2 crystal obtained with different analysis methods*

Sampling rate (MHz)	Resolution with measured integral (%)	Resolution with fitted integral (%)
100	15.3	15.0
200	13.2	12.1
500	13.0	10.9
1000	12.7	10.8

*Measured with a ^{60}Co source and averaging the resolution values of both peaks.

convoluted fit functions and for different integration intervals. It is obvious that the integration range has to be chosen properly for reproducing the signal area and that the exponential fit function works better than the convoluted solution of Eq. (3). Moreover, the signal area determined via the fit functions appears to be systematically lower than the areas obtained by integration. This holds both for BaF_2 and for CeF_3 and seems to be correlated with the sampling properties of the FADC and with the structure of the electronic noise.

The linearity of the FADC was tested by using a set of radioactive sources (^{24}Na, ^{60}Co, ^{137}Cs, and $^{238}Pu/^{13}C$). At low counting rates of $\leqslant$100 events per second the integral non-linearity was found to be less than 1% [21], probably due to baseline shifts [22–24]. The effect of the sampling rate on the energy resolution of the BaF_2 crystal was investigated between 100 MegaSample/s and 1 GS/s using a ^{60}Co source. The results (Fig. 5 and Table 4) confirm that a high sampling rate is necessary to achieve good energy resolution and that the fitting method is clearly superior in this respect. At 1 GS/s and using the fitting method the energy resolution is comparable with the performance of a standard ADC [7], whereas it falls short by 40% at 100 MS/s. A detailed study of the energy resolution as function of the γ-ray energy is performed in Ref. [21].

The time-of-flight resolution is also directly correlated with the sampling rate [23–25]. At typical rates of 500 MS/s or 1 GS/s, the resolution is 2 and 1 ns per sample, respectively, but can be improved by means of the fitting method. The time resolution that is achieved with conventional electronics can be met only with higher sampling rates of 5 GS/s. However, since the resolution in neutron energy is dominated by the time spread of the primary beam and especially by the uncertainties in the flight path [23–25], the use of FADCs is adequate in most neutron capture experiments as demonstrated in Ref. [26]. A more accurate assessment of the intrinsic time resolution of FADCs would require a dedicated study that is outside the scope of this paper [25].

Analysis of the CeF_3 signals with the fitting method showed that the additional integration by the TFA helps to improve the performance considerably (Fig. 5). This confirms that the fitting procedure can be reliably applied if

the signals do not show strong fluctuations, noise or other instabilities. Given the small size of the present CeF_3 crystal, a detailed study of the energy resolution appears premature, since the resolution may strongly depend not only on the number of photoelectrons but also on the dimensions of the crystal, the choice of the photomultiplier, and the characteristics of the TFA. A comparison with BaF_2 will be more useful when comparably large crystals become available.

4.2. Particle identification

The main background in measurements with heavy inorganic scintillators is due to γ-rays, which are produced by neutrons scattered in the sample and captured by the Ba or Ce isotopes of the scintillator. This γ background can only be discriminated via differences in the sum-energy of the respective γ cascades [8].

A minor, but not negligible contribution to the background in BaF_2 crystals is due to α-decay of the radium impurities and of their daughters. These signals differ from γ-induced events by the absence of the fast component (Fig. 1). The most common procedure for α/γ discrimination is achieved by plotting the pulse duration, defined as the time above threshold, versus the ratio of the fast (L_{Fast}) over the slow (L_{Slow}) component of the scintillation light (Fig. 6). Particle identification via the fitting method is straightforward as discussed in Ref. [10] and equally efficient with respect to the previous approach but rather time consuming and, therefore, not suited for the analysis of a large amount of raw data.

Finally, we did not observe any neutron signal in the measurements performed with the neutron beam. Especially for neutron energies below 300 keV, the neutron reactions (elastic, inelastic and capture) inside the crystals produce either typical γ-ray signals or neutron signals below the threshold.

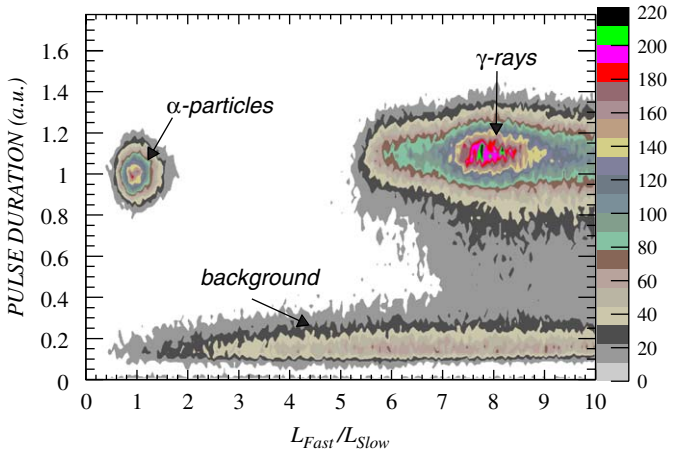

Fig. 6. Signal length (defined as the time above threshold) versus the ratio of the fast and slow component. The α-particles are emitted from a ^{214}Po source.

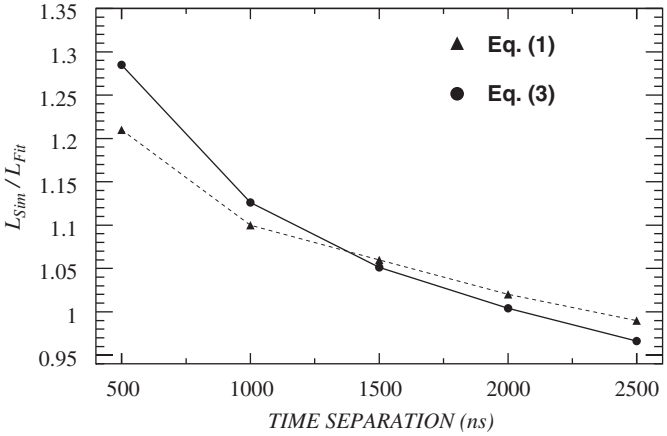

Fig. 7. Ratio of the areas of the simulated pile-up event and the fitted value as a function of the time separation between two BaF_2 signals.

4.3. Pile-up events

The possibility for resolving pile-up events was investigated by arbitrarily summing two randomly chosen BaF_2 signals sample by sample with different time shifts between the signals. The minimum distance for a correct resolution of the two pulses was then evaluated with respect to the peak position. The first pulse was reconstructed by a fit of the time interval before the start of second pulse. The reconstructed tail of the first pulse was then subtracted from the pile-up signal to isolate and to fit the second pulse.

This procedure was checked by comparing the areas of the reconstructed pulses with the original ones (Fig. 7). A good reconstruction of the two signals is obtained for time differences larger than 500 ns.

For CeF_3 the pile-up problem is less stringent because of the shorter signals. In principle, the same procedure can be applied for obtaining the corresponding corrections.

4.4. Data processing

The amount of data produced by FADC systems is huge and increases almost linearly with the counting rate. Apart from the computer time required for acquisition, transfer, and storage of the data, the time required for processing the raw data hampers a quick analysis during the experiment as well as the repeated processing of the entire data set. Quantitative estimates of the acquisition rate in typical n_TOF experiments and a description of suited hardware techniques to reduce the amount of data can be found in Ref. [27]. In this context, the fitting method provides a viable tool for fast data processing, since each signal can be characterized with only a few parameters. The raw data need to be processed only once to create the data stream tapes containing the most relevant information such as particle type, charge, time-of-flight, etc.

The CPU time required per signal has been measured for the general analysis method described in Section 3.1 and for the fitting method using Eq. (1) in order to provide an

Table 5
Comparison of CPU times required for different analysis of BaF_2 signals

Fit function	Fixed parameters	CPU time (ms)
General	—	5.4 ± 1.0
Eq. (1)	τ_s	14.2 ± 3.1
Eq. (1)	—	24.5 ± 7.9

In the first case, the CPU time employed by the general analysis algorithm (see Section 3.1) is reported. The fitting method is applied using the Eq. (1) fixing the parameter τ_s. In the last case, A_s and τ_s are left free to vary.

estimate for the processing time of the raw data. This estimate does not include the time required by auxiliary equipment, i.e. for reading and writing the data on the hard drives, bus speed, and memory. The results obtained from the analysis of BaF_2 signals using Eq. (1) are summarized in Table 5. It is evident that the application of the fitting procedure is more time consuming than the standard analysis. In particular, the use of a larger number of free parameters increases the CPU time linearly and affects the processing much more than the time duration of the pulse and/or the length of the fitting range (Table 5). Tests with other CPUs (e.g. a PIII 900 MHz) have confirmed that the required time for both algorithms is almost inversely proportional to the speed of the CPU.

According to these results, a data set containing 10^8 signals, which is recorded in a typical measurement with the 4π BaF_2 calorimeters at n_TOF [27] (42 crystals) or at DANCE (160 crystals), can be processed with a 2 GHz CPU in about 20 days.

5. Conclusions

We have compared the performance of the fitting method for analyzing the digitized signals from BaF_2 and CeF_3 scintillators with a schematic general method. The physical quantities related to the characteristics of the set-up, i.e. light output, decay time of the scintillation light, and photomultiplier properties, could be well reproduced by both approaches. The procedures were shown to work well with fit functions containing few free parameters and to provide safe particle identification and a reliable reconstruction of pile-up events.

The analytical description of the slow part of the scintillation light in BaF_2 is still hampered by the limited dynamic range of the FADC (8 bits). Currently a series of measurements has been performed at Charles University in Prague in order to improve the decay times of the scintillation light from BaF_2, to study the differential linearity of FADCs, and to understand the causes of fluctuations induced by the electronics, the temperature, etc. These studies will help to determine the best operating conditions for the combination of heavy inorganic scintillators and FADCs, and will provide information for further improvements of the analysis procedures.

Acknowledgments

S.M. acknowledges the warm hospitality of the colleagues at LANL. This work has benefited from support by Los Alamos Neutron Science Center at the Los Alamos National Laboratory, which is funded by the US Department of Energy and operated by the University of California under Contract W-7405-ENG-36, and from support by the EC under contract FIKW-CT-2000-00107 within the framework of the n_TOF-ND-ADS project.

References

[1] C. Rubbia, et al., CERN/AT/95-53, 1995.
[2] F. Käppeler, Prog. Nucl. Part. Phys. 43 (1999) 419.
[3] R. Capote, A. Ventura, F. Cannata, J.M. Quesada, Phys. Rev. C 71 (2005) 06432.
[4] Acqiris, website: ⟨http://www.acqiris.com⟩.
[5] n_TOF Collaboration, Report INTC-2003-036, CERN, Switzerland, 2003.
[6] M. Heil, et al., Report LA-UR-99-4046, Los Alamos National Laboratory, 1999.
[7] K. Wisshak, et al., Nucl. Instr. and Meth. A 292 (1990) 595.
[8] M. Heil, et al., Nucl. Instr. and Meth. A 459 (2001) 229.
[9] C.W.E. van Eijk, Nucl. Instr. and Meth. A 460 (2001) 1.
[10] S. Marrone, et al., Nucl. Instr. and Meth. A 490 (2002) 299.
[11] N.V. Kornilov, et al., Nucl. Instr. and Meth. A 497 (2003) 467.
[12] S.D. Jastaniah, P.J. Sellin, IEEE Trans. Nucl. Sci. NS-49 (2002) 1824.
[13] S.D. Jastaniah, P.J. Sellin, Nucl. Instr. and Meth. A 517 (2004) 202.
[14] Q. Yue, et al., Nucl. Instr. and Meth. A 511 (2003) 408.
[15] Electron Tubes Ltd., website: ⟨http://www.electron-tubes.co.uk⟩.
[16] Photonis Group, website: ⟨http://www.photonis.com⟩.
[17] ROOT, Manual and Class References available on website: ⟨http://root.cern.ch⟩.
[18] F. James, MINUIT, CERN Program Library Long Writeup D506, CERN Geneva, 1994.
[19] G.F. Knoll, Radiation Detection and Measurement. 2nd ed. Section 9-VII.
[20] Anon., Photomultiplier Tubes, Philips Photonics, Brive, France, 1994 Section 2.2.
[21] R. Terlizzi, Ph. D. Thesis, Università di Bari, April 2006.
[22] A. Laptev, et al., Nucl. Instr. and Meth. A 543 (2005) 502.
[23] L. Bardelli, G. Poggi, Nucl. Instr. and Meth. A. 560 (2006) 517.
[24] L. Bardelli, G. Poggi, Nucl. Instr. and Meth. A. 560 (2006) 524.
[25] J. Nissilä, et al., Nucl. Instr. and Meth. A 538 (2005) 778.
[26] G. Lorusso, et al., Nucl. Instr. and Meth. A 532 (2004) 622.
[27] U. Abbondanno, et al., Nucl. Instr. and Meth. A 538 (2005) 692.